HAL
open science

Influence of the Spark Plasma Sintering temperature on the structure and dielectric properties of BaTi(1-x)ZrxO3 ceramics

Blessing N. Ezealigo, Roberto Orrù, Catherine Elissalde, Hélène Debéda, U-Chan Chung, Mario Maglione, Giacomo Cao

To cite this version:

Blessing N. Ezealigo, Roberto Orrù, Catherine Elissalde, Hélène Debéda, U-Chan Chung, et al.. Influence of the Spark Plasma Sintering temperature on the structure and dielectric properties of BaTi(1-x)ZrxO3 ceramics. Ceramics International, 2021, 47 (3), pp.3614-3625. 10.1016/j.ceramint.2020.09.210 . hal-02978411

HAL Id: hal-02978411

https://hal.science/hal-02978411v1

Submitted on 26 Oct 2020

HAL is a multi-disciplinary open access archive for the deposit and dissemination of scientific research documents, whether they are published or not. The documents may come from teaching and research institutions in France or abroad, or from public or private research centers.

L'archive ouverte pluridisciplinaire **HAL**, est destinée au dépôt et à la diffusion de documents scientifiques de niveau recherche, publiés ou non, émanant des établissements d'enseignement et de recherche français ou étrangers, des laboratoires publics ou privés.

Influence of the Spark Plasma Sintering temperature on the structure and dielectric properties of $BaTi_{(1-x)}Zr_xO_3$ ceramics

Blessing N. Ezealigo[1], Roberto Orrù[1,*], Catherine Elissalde[2,*], Hélène Debéda[3], U-Chan Chung[2], Mario Maglione[2], Giacomo Cao[1]

[1]*Dipartimento di Ingegneria Meccanica, Chimica e dei Materiali, Unità di Ricerca del Consorzio Interuniversitario Nazionale per la Scienza e Tecnologia dei Materiali (INSTM) - Università degli Studi di Cagliari, via Marengo 2, 09123 Cagliari, Italy*

[2]*Université de Bordeaux, CNRS, ICMCB, UMR 5026, 87 avenue du Dr A. Schweitzer, 33608 Pessac, France*

[3]*Université de Bordeaux, Laboratoire IMS, UMR 5218, 351 Cours de la Libération, 33405 Talence, Cedex, France*

(*) Author to whom all correspondence should be addressed

Revised unmarked paper

September 2020

Abstract

In this work, structural and dielectric properties of $BaTi_{(1-x)}Zr_xO_3$ (BTZ) ceramics prepared by Spark Plasma Sintering (SPS) from powders obtained via Self-propagating High-temperature Synthesis (SHS) are shown to be strongly affected by the sintering temperature. In addition, a post-annealing treatment in air of the as-prepared ceramics leads to a transition from the hexagonal to the tetragonal and cubic phases. The SPS ceramics corresponding to compositions $0.05 \leq x \leq 0.20$ and obtained at a sintering temperature of 1200°C exhibit a standard ferroelectric behavior. In contrast, a diffuse phase transition is observed for the case of ceramics sintered at higher temperatures. Finally, the BTZ ceramic containing 5 at.% of Zr displays the best dielectric permittivity and piezoelectric properties as compared to the other compositions taken into account.

Keyword: Dielectric permittivity, spark plasma sintering, piezoelectric, post-annealing; self-propagating high-temperature synthesis.

Corresponding authors: roberto.orru@dimcm.unica.it, catherine.elissalde@icmcb.cnrs.fr

1. Introduction

To meet specific applications, the strategy commonly adopted by the scientific community to improve the electrical characteristics of ABO_3 perovskite materials is to change the ceramics' chemical content. Indeed, the substitution of the A or B cation sites with other isovalent ions can modify the material's dielectric properties, and lead to changes in the related transition temperatures as well as the formation of specific phases **[1]**. In this context, zirconium substituted barium titanate (BTZ) has attracted great attention in the last decade because of its wide range of applications, owing to its improved properties and potential to replace lead-based ferroelectric materials **[2-3]**. These properties include high dielectric permittivity, relatively low dielectric loss, large voltage tunability of the dielectric permittivity, good chemical stability, and attractive lead-free relaxor behavior **[4-6]**.

In this regard, the marked influence of Ti sites substitution with Zr on the properties of the resulting BTZ ceramics obtained by conventional sintering has been addressed by various authors **[7-9]**. The BZT potential for application in tunable microwave devices has been demonstrated **[10]**. Specifically, it is reported that, when the amount of Zr content is within the range $0 \leq x \leq 0.10$, the ceramics show a classical ferroelectric behavior **[9, 11]**. However, at higher Zr content, the ferroelectric phase coexists with the paraelectric one, leading to a diffuse phase transition. The latter one is promoted by the energy difference between the ferroelectric and the paraelectric phases **[12]**. Furthermore, the classical ferroelectric transitions of $BaTiO_3$ continuously give rise to diffuse phase transition ($0.10 < x \leq 0.26$) and relaxor state ($0.26 < x \leq 0.40$), whose temperature of occurrence decreases to low values as the Zr content increases **[13]**. It is worth to mention that, in addition to the latter finding, the phase transition can also be influenced by temperature variation, depolarization due to presence of porosity, slight changes in the chemical potential, and

grain size effect **[12, 14-15]**. A high dielectric permittivity of about 14,000 has been reported for dense BTZ ceramics (x=0.08), which were produced by solid state reaction using high energy milling followed by conventional sintering **[9]**.

Among the synthesis methods proposed to obtain BTZ powders, Sol-gel **[16-17]**, Sol-gel based Pechini method **[18]**, solid-state reactions **[19-20]**, and combustion synthesis **[21-22]** are reported. The formation of BTZ solid solution is obtained by conventional sintering in the temperature range 1300−1450°C after 2−10 h treatment. In addition to conventional sintering, only few studies have also been conducted on BTZ ceramics using Spark Plasma Sintering (SPS) **[23-25]**. The latter one is an efficient sintering process where powders are rapidly heated by Joule effect, due to the combination of pulsed electric current and the application of uniaxial mechanical pressure **[26]**. In particular, the structure and electromechanical properties of $Ba(Zr_{0.2}Ti_{0.8})O_3$ ceramics obtained by SPS at 1100°C and subsequently annealed at 1000−1400°C for 12h has been investigated by Maiwa **[23, 27]**.

In this work, SHS and SPS techniques are combined for the first time for the preparation of Zr-substituted barium titanate ceramics ($BaTi_{(1-x)}Zr_xO_3$). Briefly, SHS is a combustion synthesis method based on the local ignition of highly exothermic reactions which can self-propagate without additional energy supply **[28-29]**. Temperatures in the range 2000−5000 K and cooling rates up to 10^3 K/min can be reached during SHS and, more importantly, high-purity products can be correspondingly obtained in a very short time (order of seconds) **[28]**.

The present work is aimed to produce single-phase $BaTi_{(1-x)}Zr_xO_3$ (x=0.05−0.25) ceramics by combining the two fast processes mentioned above, i.e. by following the so-called SHS-SPS approach. The influence of the sintering temperature (T_D) on density, composition (structure), dielectric, and piezoelectric properties of SHS-SPS ceramics is systematically investigated. The

optimal SPS, as well as post-annealing, conditions, are then identified. A novel procedure of tuning the dielectric response of the BTZ ceramics by varying the sintering temperature, regardless of the Zr content, is presented.

2. Experimental

BTZ powders were prepared by SHS according to the following chemical equation:

$$2BaO_2 + (1\text{-}2x)TiO_2 + 2xZrO_2 + Ti \rightarrow 2BaTi_{(1-x)}Zr_xO_3 \quad (1)$$

Hereto after, the $BaZr_{0.05}Ti_{0.95}O_3$, $BaZr_{0.10}Ti_{0.90}O_3$, $BaZr_{0.15}Ti_{0.85}O_3$, $BaZr_{0.20}Ti_{0.80}O_3$, and $BaZr_{0.25}Ti_{0.75}O_3$ compositions will be indicated as BTZ005, BTZ010, BTZ015, BTZ020, and BTZ025, respectively. Details on the synthesis of the precursors and procedure can be found in **[30]**.

The SHS products were first converted into powders after 20 min ball milling treatment using a SPEX 8000 mixer mill (SPEX CertiPrep, Metuchen, NJ, USA). It is worth to mention that such a mild milling conditions (the ball to powder weight ratio was only equal to 2) are not expected to modify the grain size of SHS product and, in turn, affect the microstructure of the sintered ceramics.

Subsequently, 3g of the resulting powders were consolidated by SPS (515S model, Fuji Electronic Industrial Co., Ltd., Kanagawa, Japan) under vacuum conditions (down to 20 Pa) and sintering temperatures (T_D) in the range 1200–1400 °C (heating rate of 100°C/min and holding time of 5 min) with a mechanical pressure of 40 MPa. Graphite die of 14.7 mm inner diameter, 30 mm height, and 30 mm outer diameter was used. SPS runs were carried out under temperature-controlled mode using an optical pyrometer (IR-AHS2, Chino, Tokyo, Japan) focused on the external surface of the die. After SPS, the bulk samples were polished on their top and bottom

surfaces using progressively finer abrasive paper, to finally obtain 2 mm thick disks. The pellets were then post annealed for 3h at 1200°C (Nabertherm, mod. N60/ER, Germany) in an oxygen-rich atmosphere to re-oxidize the samples and remove the carbon contamination arising from the graphite tools.

The absolute density values of the bulk specimens were determined by the Archimedes' method using distilled water as immersion medium. The crystalline phases in both the SHS powders and the SPS specimens were identified using an X-ray diffractometer (PANalytical X'pert Pro diffractometer, Netherlands; operating at 40 kV and 40 mA, using the X'Celerator detector) equipped with a Ni filtered CuKα radiation (λ = 1.5405 Å). The relative content of the different phases was determined taking advantage of a Rietveld analytical procedure **[31]**.

Fracture surfaces of BTZ ceramics were examined by high resolution scanning electron microscopy (HRSEM) (mod. S4000, Hitachi, Tokyo, Japan) equipped with a UltraDry EDS Detector (Thermo Fisher Scientific, Waltham, MA, USA). Microstructural analysis (grain size, porosity) were conducted on SEM images using the open source software Image J (version 1.54a for Windows, 64 bit, National Institutes of Health, Bethesda, MD, USA).

The dielectric measurements were carried out after depositing by sputtering gold electrodes on both sides of the dense ceramics (Technics Hummer JR, USA). The LCR meter (Wayne Kerr 4300, London) recorded the capacitance and imaginary permittivity (ε_i) values from which the data acquisition program estimated the dielectric permittivity and dielectric loss. Liquid nitrogen was used to decrease the set-up temperature to about 85 K and a furnace (Eurotherm 3508, UK) raised the temperature to 450K which was measured using a K-type thermocouple. For the sake of reproducibility, each experiment was repeated at least twice.

Regarding the measurement of the piezoelectric properties, the samples were poled at a high voltage of about 2 kV (10 kV/cm) generated by a suitable supply (AET technologies, France) at 80°C under Nitrogen gas in a furnace (AET technologies, France). The applied field was kept during sample's cooling. The resonance (f_r) and anti-resonance (f_a) frequencies from which the electromechanical parameters were estimated, have been obtained using a network analyzer (Agilent technologies E5061B, USA).

3. Results

3.1 SHS powders of Zr substituted $BaTiO_3$

The five BTZ compositions investigated in the present work all display a self-propagating character, i.e. the reaction occurred spontaneously after initiation without additional energy, regardless of the Zr content. The XRD patterns of the resulting SHS products, after being milled to powders, are shown in **Fig. 1.**

The hexagonal $BaTiO_3$ phase is the only one (matched with the JCPDS card reference pattern mentioned in **Fig. 1**) detected by this analysis for x=0.05 and 0.10. Also, some peaks identified as *c* $BaZrO_3$ and *t* BTZ appear in the XRD patterns of SHS products obtained for larger Zr content (x>0.10). Moreover, their intensity, and in particular that one of the main peak corresponding to the cubic $BaZrO_3$ phase, progressively increase as the x value is augmented. It is important to note that in the powders synthesized by SHS, the desired single phase BTZ was not achieved (**Fig. 1**), rather an additional $BaZrO_3$ phase was formed, which implies that at this stage Zr is yet to be fully substituted in the B site of the $BaTiO_3$ lattice.

In this regard, it is interesting to compare the composition and structure of BTZ powders obtained by SHS (**Fig. 1**) with those ones reported in the literature for analogous products prepared

by calcination [**20, 32-33]**. The compositional/structural characteristics of $BaTi_{(1-x)}Zr_xO_3$ products synthesized by calcination are found to depend on the x value. For instance, a tetragonal perovskite phase was obtained by Badapanda et al. **[33]** for BTZ005 powders calcined at 1100°C for 4h after 5h milling. On the other hand, BTZ015 powders calcinated for 4h at 1200°C after milling the reactants for 5h, lead to a single-phase cubic perovskite structure **[20]**. Similarly, Rout et al. **[32]** obtained a perovskite cubic BTZ025 phase after 4h calcination at 1350°C of powders subjected to repeated cycles of mixing and grinding.

The diverse outcomes resulting from the two synthesis methods can be motivated as follows. The formation of the metastable hexagonal phase, which is not detected in calcinated powders, could be explained by the peculiar characteristics (i.e. process rapidity, high temperatures, heating and, above all, cooling rates) of the SHS method, which evolves quite far from the equilibrium conditions. Therefore, metastable phases could be retained at room temperature. In addition, the intense milling treatments performed when considering the calcination method [**20,32-33]** certainly promote diffusion phenomena involved in the synthesis process, so that the formation of single-phase products is favored.

As mentioned in the Experimental section, in the present work the SHS products are mildly ball milled just to generate powders to be processed by SPS. Nonetheless, the effect of a more intense milling treatment on SHS powder and the resulting bulk BZT products characteristics will be the subject of a research work currently in progress.

3.2 Spark Plasma Sintering of SHS powders

The powders synthesized by SHS were then processed by SPS (5 min, 40 MPa, 100°C/min). The influence of the sintering temperature on the composition can be observed from

room temperature XRD results depicted in (**Fig. 2)**. Specifically, the XRD patterns of the bulk samples for the five BTZ systems are compared in **Fig. 2(a)-(b)** for two selected sintering temperatures 1200°C and 1400°C, respectively. It is important to note that XRD data for Zr-substituted $BaTiO_3$ powders sintered at T_D=1300°C are very similar to those ones obtained at 1400°C, hence they are not reported here.

The XRD patterns evidence that, regardless of the Zr content, the *h* $BaTiO_3$ originally present in SHS powders undergoes a gradual structural (phase) transformation during SPS. Specifically, this effect is more pronounced as the dwell temperature is increased from 1200 to 1400°C. Nonetheless, when considering the composition corresponding to x=0.05, the original hexagonal phase is still significantly present in the sintered ceramic. A direct indication of the phase transformation observed when x increases is provided, for example, by the intensity of the *h* $BaTiO_3$ peak which falls in the range $26° \leq 2\theta \leq 27°$. Such peak decreases and tends to disappear, particularly when T_D=1400°C. XRD analysis also evidences that, when the sintering process is performed at 1400°C, the intensity of the *c* $BaZrO_3$ and the *h* $BaTiO_3$ peaks are also markedly reduced with respect to the starting SHS powders (**Fig. 1**). It is thus possible to conclude that, depending on the x value, the content of *t* BTZ or the *c* BTZ phases is enhanced (**Fig. 2(b)**) during SPS when the sintering temperature is high enough. This is confirmed by the shift in 2θ diffraction peak at about 31° towards a lower angle (**Fig. 2(c)**). However, a residual presence of *c* $BaZrO_3$ is still detected by XRD. In the literature, the tetragonal phase is generally reported for $x \leq 0.08$ **[8, 34]** while the cubic and/or rhombohedral phases are found for $x \geq 0.10$ **[18, 20, 35-36]**.

3.3 Post-annealing of SPS samples

From the results described in *section 3.2*, it is found that the bulk specimens obtained by SPS still contain undesired secondary phases, particularly *h* $BaTiO_3$ and/or *c* $BaZrO_3$, whatever the Zr content. The effect of a post-heat treatment in air, conducted for 3 h at 1200°C, on the composition of the BTZ ceramics produced by SPS at T_D= 1200, 1300, and 1400°C, was then investigated. The room temperature XRD patterns of the corresponding post-annealed samples are shown in **Fig. 3(a)-3(b)**, for the compositions corresponding to *x*=0.05 and 0.25, i.e. the lowest and highest Zr content examined in this work.

Let us consider first the ceramics obtained with the lowest Zr content (**Fig. 3(a)-3(b))**. The post-annealing treatment appears to remove the *h* $BaTiO_3$ phase initially present in SPS sintered products (**Fig. 2(a)-2(b)**). Also, *t* BTZ is the major phase detected by XRD at room temperature in post-thermal treated SPS ceramics obtained at T_D=1200 and 1300°C. In particular, the Rietveld analysis **(**see Supplementary **Table S1**) revealed that, after the post-annealing process, the sintered product obtained by SPS at T_D= 1200°C is mainly composed of the P4mm tetragonal phase (about 87 wt. %) with a small amount of the cubic Pm-3m phase (approximately 13 wt.%). As the sintering temperature was augmented to 1400°C, the content of the cubic phase in the post-annealed ceramic increased at the expenses of the tetragonal one. Nonetheless, based on the Rietveld analysis, the BTZ005 sample obtained for T_D= 1400°C still consists of a mixture of tetragonal P4mm (about 70 wt.%) and Pm-3m (about 30 wt.%) phases (see Supplementary **Table S1**). The phases' coexistence could arise from the segregation of Zr when high sintering temperature (1400°C) is applied on heterogeneous starting powders. As a result, ceramics containing Zr rich (cubic) and Zr poor (tetragonal) phases could be obtained **[37]**.

XRD data of post-annealed SPS samples corresponding to x=0.25 are shown in **Fig. 3(c)**. Residual $BaZrO_3$ is reduced during post heat treatment in air, to finally provide single-phase *c* BTZ for ceramics processed by SPS at T_D=1400°C, as confirmed by the Rietveld analysis (see Supplementary **Table S1**). It should be noted that the compositional changes observed when considering x=0.10, 0.15, and 0.20, not reported here for the sake of brevity, fall within those ones described above in the case of x=0.05 and 0.25.

Another effect observed after the post-annealing treatment is the color change of SPS samples. Indeed, as shown in **Fig. 4a**, the resulting disks are dark, after the sintering process.

Regarding the latter finding, it should be noted that the dark color in barium titanate- as well as other oxide-based ceramics is general observed when the related synthesis and/or sintering processes are conducted under reducing environments. In the present work, both the SHS and SPS routes were performed under such condition. As far as the SHS powders are concerned, it was recently shown that their dark color is due to the fact that the synthesized products are oxygen deficient **[30]**. In addition, a heat-treatment of these powders in air at increasing temperatures (up to 1200 °C) was found to determine a gradual color change from the initial dark to light yellow **[30]**. The same motivation is also valid to justify the dark color of bulk BTZ samples obtained in this work by SPS, since the adopted reducing conditions (vacuum) likely lead to the formation of oxygen vacancy. Accordingly, in order to restore the expected BTZ stoichiometry and also make the obtained ceramics insulating, a post-annealing treatment in air was carried out. The latter process performed at various temperature/time conditions evidences that, at relatively lower temperatures (800–1000°C), the samples exhibited several cracks on their surface, and the transformation from dark to white color was not obtained. In contrast, such drawback was avoided, or strongly limited, when the annealing process was conducted for 3 h at 1200°C. The optical

images of the various BTZ samples correspondingly obtained are shown in **Fig. 4b**. The annealing process induces a significant color change from dark to white-grey in all BTZ ceramics. Thus, a post-annealing at 1200°C for 3h appears as the optimal condition to be adopted.

3.4 Microstructural characterizations

SEM images of the fracture surfaces of BTZ005 and BTZ025 ceramics obtained by SPS at T_D=1200 and 1400° and annealed at 1200°C for 3h are shown in **Fig. 5(a)-5(d)**. The densities of post-annealed ceramics are reported in **Fig. S1 (Suppl. material)**.

BTZ005 sintered at 1200°C exhibits an inhomogeneous microstructure with several dense zones made of grains with a melted aspect that make an accurate evaluation of the corresponding grain size difficult (**Fig.5a**). These areas are still present in ceramics sintered at 1400°C, while the microstructure is globally more homogeneous with well-defined grains and grain boundaries (**Fig.5b**). The observed transgranular fracture mode reflects weak grain boundaries. As far as the more homogeneous region of the BTZ005 sample sintered at 1400°C is concerned, grain size estimated using Image J software **[38]** is in the range 2–4 µm, so that no exaggerated grain growth is observed despite the high sintering temperature. The microstructure of BTZ025 ceramics sintered at 1200°C is characterized by a significant level of porosity and the presence of cracks (**Fig.5c**). This agrees with the low value of density obtained (**Fig. S1**). Similar to BTZ005, when the sintering temperature is increased up to 1400°C, the microstructure becomes denser, in good agreement with the values reported in **Fig. S1**. The fracture remains transgranular and equiaxed grains in the size range 1–3 µm are observed. As previously mentioned for the BTZ005 product sintered at 1400°C, the corresponding grain size values were also estimated by considering the more homogeneous BTZ025 sample region where grain boundaries can be clearly identified.

3.5 Dielectric study

3.5.1 Effect of sintering temperature on dielectric behavior

The variation of the dielectric permittivity as a function of temperature for the BTZ ceramics sintered at different T_D and post-annealed for 3h at 1200ºC are shown in **Fig. 6.**

For a fixed composition, both the permittivity values and the transition temperatures are affected by the sintering temperature. Higher T_D leads to a decrease of the temperature corresponding to the maximum of permittivity value (T_m) as well as an increase in permittivity levels, especially in the vicinity of the transition (**Fig. 7; Table S2 (Suppl. Material**)). In particular, it is worth noting that, for the composition corresponding to x= 0.05, a sintering temperature increase from 1200°C to 1400°C also induces a change from a classical ferroelectric to a more diffuse phase transition. A decrease of the Curie Temperature and an increase of the Rhombohedral (R)–Orthorhombic (O) [R–O] and Orthorhombic (O)–Tetragonal (T) [O–T] phase transitions were correspondingly observed. When the Zr content is increased, the transition temperature is decreased, as expected, and for ceramics sintered at temperatures higher than 1200°C, the ferroelectric behavior changes from classical (x=0.05) to a diffuse mode (x>0.10). The dielectric study as a function of temperature (**Fig. 6**) confirms the diffuse (not relaxor) behavior of the BTZ ceramics obtained by SHS-SPS, due to the absence shift in T_m as a function of frequency for $0.05 \leq x < 0.20$ (**Fig. S2 (Suppl. Material))**. Whatever the Zr content and the sintering temperature, the dielectric loss at 1 kHz remains stable and mostly lower than 8%. The comparison of dielectric behavior with regards to T_D for each Zr composition is shown in **Fig. S3 (Suppl. Material)**.

To investigate the behavior in the paraelectric region, the Curie constant, *C*, was estimated from the Curie-Weiss law:

$$\varepsilon = \frac{C}{(T - T_o)}\ ;\ (T>T_c) \qquad (2)$$

where T_c is the Curie point (transition temperature).

The inverse of the dielectric permittivity (1/ε) plotted as a function of temperature was used to estimate the Curie-Weiss temperature (T_o) and the Curie constant **Fig. 8** and **Table S3 (Suppl. Material).**

Regarding the investigated range of Zr content, the Curie constant decreases monotonically with an increase of the *x* value for a given T_D. Also, the Curie-Weiss temperature was found to decrease with T_D and Zr content.

The modified Curie-Weiss (C-W) plot can be used to describe the deviation from linearity due to the diffuse character of the transition. The modified Curie-Weiss equation is given by:

$$\frac{1}{\varepsilon} - \frac{1}{\varepsilon_m} = \frac{(T - T_m)^{\gamma}}{C}\ ;\ (T>T_m) \qquad (3)$$

where ε is the real permittivity, ε_m is the maximum dielectric constant, T_m is the temperature at the maximum dielectric permittivity, γ is the diffuseness coefficient. For normal ferroelectrics γ=1, while for relaxor γ=2.

The modified Curie-Weiss plots and the corresponding data are provided in **Fig. S4** and **Table S3 (Suppl. Material)**, respectively.

To illustrate the change of behavior from classical to diffuse one as a function of the Zr content, the variation of T_c (T_m) and diffuseness coefficient are presented in **Fig. 9** for ceramics sintered at 1400°C.

3.6 Piezoelectric study

In **Fig. 10** the results of the piezoelectric study of BTZ are presented. The piezoelectric charge coefficient (d_{31}) and the planar electromechanical coupling factor (k_p) were significantly influenced by the SPS temperature (T_D). All samples show good mechanical quality factor (Q_m), consistent with the low dielectric loss (see Supplementary **Table S4)**. A graph showing impedance as a function of frequency, from which resonance and antiresonance frequencies can be obtained, is reported in **Fig S5 (Supp. Material**) for the case of BTZ005 ceramics sintered at 1300°C.

BTZ025 samples could not be poled due to high current leakage arising from their low density. Hence, no piezoelectric data were obtained for this system. The following equations were used to obtain the electromechanical parameters **[41]**:

$$Q_m = \frac{1}{2\pi f_r Z_m C}\left(\frac{f_a^{\,2}}{f_a^{\,2} - f_r^{\,2}}\right) \tag{4}$$

$$k_p \approx \frac{f_a^2 - f_r^2}{f_a}, \tag{5}$$

$$k_{31} = \sqrt{\frac{\pi}{2}\frac{f_a}{f_r}\frac{1}{\frac{\pi}{2}\frac{f_a}{f_r} - \tan\left(\frac{\pi}{2}\frac{f_a}{f_r}\right)}}, \tag{6}$$

$$s_{11}^E = \frac{1}{4\rho f_r^{\,2} w^2}, \tag{7}$$

$$d_{31} = k_{31}\sqrt{\varepsilon\, s_{11}^E}, \tag{8}$$

where, in addition to the parameters (d_{31}, k_p, and Q_m) previously defined, f_r, f_a, Z_m, C, k_{31}, , s_{11}^E, ε, ρ, and w are resonance frequency, anti-resonance frequency, minimum impedance, Capacitance (in Farads), electromechanical coupling factor in the length extensional mode, elastic coefficient

at constant electric field, dielectric permittivity at room temperature, density in Kg/m^3, and width of the ceramics, respectively.

4 Discussion

4.1 Structural analysis of BTZ ceramics: from SHS powders to SPS and post-annealed samples. Evolution of their composition

The presence of the high-temperature stable *h* $BaTiO_3$ phase in the SHS product with a small contribution of peaks attributed to *t* BTZ is likely ascribed to the severe processing conditions (high temperature, heating, and cooling rates) inherent to the synthesis process as well as to the reducing environment (Argon gas) correspondingly adopted. The additional *c* $BaZrO_3$ phase is also detected at Zr content ≥ 15 wt.%, i.e. (BTZ015, BTZ020, and BTZ025), proving that a solid solution has not formed between the $BaTiO_3$ and $BaZrO_3$ phases, while a co-existence of the individual phases is obtained. When $x \leq 0.10$, no $BaZrO_3$ phase was detected due to the low concentration of Zr. It should be noted that the detailed quantitative analysis of the XRD pattern (Rietveld method) for the BTZ015 powder also evidenced the presence of a small amount of *c* $BaTiO_3$ along with traces of Ba_2TiO_4 **[30]**. Nonetheless, due to the relatively low intensity of the corresponding peaks, these two phases cannot be unequivocally identified in the XRD patterns shown in **Fig. 1**, so that they are not considered in the present work.

After SPS, a decrease in the *h* $BaTiO_3$ peak intensity is observed with respect to the starting SHS powders. Moreover, according to the Zr content, the *h* $BaTiO_3$ phase is gradually transformed into *t* BTZ or *c* BTZ, as the T_D value is progressively increased. The formation of *c* BTZ phase is favored by higher Zr amounts and when the sintering temperature is set to 1400ºC (**Fig. 2b-2c**). Twofold effects are noticeable for both the highest Zr content (i.e x=0.25) and sintering temperature (i.e. T_D=1400°C), respectively: the formation of the *c* BTZ phase concomitant with the disappearance of *t* BTZ. In parallel, the secondary *c* $BaZrO_3$ phase (c BZ) decreases progressively as the sintering temperature is increased from 1200 to 1400°C. The overall XRD

study shows that the targeted $BaTi_{(1-x)}Zr_xO_3$ solid solution can only be obtained by SHS-SPS under specific composition and temperature conditions. A high-temperature treatment of the SPS product is required to obtain the targeted single-phase BTZ.

The decisive role of the post-annealing treatment on the evolution of the phases present in SPS ceramics is emphasized here. Beyond its re-oxidizing role, post-annealing, when performed at sufficiently high temperature, allows for the elimination of the *h* $BaTiO_3$ phase still present in some of the SPS ceramics. However, it should be noted that, during the post-annealing process, the hexagonal and tetragonal phases are partially or fully converted into the cubic one (Supplementary **Table S1**). This finding agrees with the work of Jha and Jha **[42]** focused on $BaZr_{0.05}Ti_{0.95}O_3$ ceramics obtained by conventional technique, where the sintering process conducted at higher temperatures caused the tetragonal to cubic phase transformation. The formation of the *c* BTZ phase for Zr content corresponding to x=0.10–0.25 is also consistent with similar results reported in the literature for BTZ ceramics obtained by conventional solid-state reactions **[36]**.

Besides, from the secondary *c* $BaZrO_3$ phase evolution, which depends on the thermal cycle, it is clear that the procedure to eliminate such unwanted secondary phase is to combine the SPS process (T_D=1400°C) with a post-thermal treatment carried out at 1200°C or higher temperatures (**Fig. 3**).

In addition, whatever the Zr content, the post-annealing must be performed at least at 1200°C to efficiently re-oxidize the samples. It is worth noting that an annealing duration of 3 h is not only efficient enough, but also much shorter than the one reported in the literature **[23, 27]**.

4.2 Dielectric behavior: Effect of sintering temperature and composition

For a fixed Zr content (x=0.05), a normal ferroelectric behavior is observed. However, for T_D =1400ºC, the Orthorhombic–Tetragonal [O–T] phase transition becomes less marked compared with ceramics obtained at $T_D \leq$1300ºC, and a broad transition is observed at T_c. This effect can be correlated with the XRD analysis that shows a transition, albeit uncomplete, from *t* BTZ to *c* BTZ, when increasing the sintering temperature. Generally, all BTZ ceramics compositions sintered at T_D =1200ºC, showed a normal ferroelectric behavior except for the x=0.25 composition. In the latter case, the very diffuse phase transition associated with low permittivity values is correlated with the low value of density obtained at 1200°C. The microstructural investigation of BTZ025 sintered at 1200°C confirms a poorly densified ceramic and the presence of cracks. It is worth noting that no significant shift in $T_{O\text{-}T}$ and T_c was observed from x= 0.05 to x= 0.20, thus demonstrating that a sintering temperature of 1200°C is not sufficient to induce the Zr-Ti substitution.

When sintering is performed at 1400°C, a continuous decrease of T_c is observed when the composition was varied from x=0.10 to x=0.25 and the transition becomes more and more diffuse. A relaxor behavior starts to be detected for x=0.25 (ΔTm = 8 from 100 Hz to 500 kHz), for which *c* BTZ is the only phase observed on the room temperature XRD pattern (**Fig. 3(c)**).

As a result, a change from classical to diffuse ferroelectric behavior in SHS-SPS ceramics can be induced by increasing not only the Zr content but also the sintering temperature at a fixed composition. Considering the microstructural analysis, such dielectric behavior is not correlated to the microstructure, while, as expected, depends rather on compositional effects at the atomic scale.

High diffusivity parameter (γ) was observed at low Zr content. The reason for this finding could be related to the coexistence of tetragonal and cubic phases seen in **Fig. 3(b)**. However, at high Zr content, the obtained γ parameter is in the range of the values reported in the literature, which generally depend on the adopted synthesis process **[35, 43-44]**. In addition, similar to the works by Mahesh et al. **[20]** and Cai et al. **[45]**, higher sintering temperature induces diffuse transition and increases the γ parameter (see Supplementary **Table S3**). The T_c (T_m) values obtained for the various compositions are in good agreement with the literature for BTZ ceramics obtained by other methods **[46-48]**.

4.3 Piezoelectric study

Both the composition and the sintering temperature have an impact on the piezoelectric performances. The piezoelectric charge coefficient decreases with increasing x values (**Fig. 10(a)**), which confirms that high Zr content does not favor the obtainment of good piezoelectric properties. This result is effectively in agreement with the improved piezoelectric properties reported for BTZ ceramics with $x \leq 0.08$ **[44, 46 47, 49]**. In addition, our study also evidenced that, when operating under optimal SPS temperature (T_D) conditions to obtain higher values of the dielectric permittivity, the piezoelectric properties are correspondingly enhanced, which is in line with results reported in the literature for BTZ ceramics produced by alternative techniques **[49-50]**.

When considering BTZ005, sintering at 1200°C results in moderate density values and poor quality of grain boundaries, that are not convenient for improving piezoelectric properties. On the other hand, BTZ005 sintered at 1300°C exhibits the optimal piezoelectric properties, which is in agreement with the literature **[39-40, 51]**. However, the obtained piezoelectric coefficient remains relatively low when compared to the state of the art **[23, 47, 51]**. Improvements based on

microstructure (density and grain size) and on the poling conditions would allow reaching better performances.

5. Conclusion

BTZ ceramics have gained a high interest due to the possibility to tailor their ferroelectric properties through a proper composition control. Different BTZ ceramics are produced in this work using a novel approach based on the combination of the fast SHS and SPS processes, followed by an air-thermal treatment of relatively short duration (3 h), compared to the annealing time (10 h) typically considered in the literature. Here, the possibility of tuning the dielectric response (from classical to diffuse phase transition or relaxor) by varying, for a given composition, the sintering temperature, was clearly evidenced. In this regard, it should be noted that, to the best of our knowledge, no study was reported so far in the literature on the influence of the SPS temperature on the dielectric behavior of BTZ ceramics, regardless of the method used for powder synthesis.

Specifically, it was observed that the T_D value and the Zr content significantly impact the structure, microstructure, dielectric, and piezoelectric properties of the SHS-SPS prepared ceramics. The $BaZrO_3$ impurity phase formed during SHS, and still present after SPS, was eliminated thanks to the post-annealing treatment of the sintered ceramics. Increasing the sintering temperature above 1200°C leads to improved density, more homogeneous microstructure, as well as enhanced dielectric permittivity. The ceramic containing 5 at.% of Zr sintered at T_D=1300ºC showed the best piezoelectric properties. Better performances are expected if a single-phase ceramic is obtained after SPS and the microstructure of the final ceramics is suitably refined. Work is underway along this direction.

Acknowledgments

One of the authors (B.N.E) performed her activity in the framework of the International PhD in Innovation Sciences and Technologies at the University of Cagliari and is also grateful for the ERASMUS Placedoc program for allowing mobility to France. The valuable contribution of Dr. S. Garroni and Dr. A. Iacomini (University of Sassari, Italy) for Rietveld's analysis and useful discussion is gratefully acknowledged.

References

[1] J.Z. Jiang, F.W. Poulsen, S. Mørup, Structure and thermal stability of nanostructured iron doped zirconia prepared by high-energy ball milling. J. Mat. Res. 14(1999)1343–1352. https://doi.org/10.1557/JMR.1999.0183.

[2] R. Potong, R. Rianyoi, A. Chaipanich, Dielectric Properties of Lead-Free Composites from 0-3 Barium Zirconate Titanate-Portland Cement Composites. Ferro. Lett. Sec., 38(2011) 18–23. https://doi.org/10.1080/07315171.2011.570176.

[3] R. Saravanan, Titanate based ceramic dielectric material, first ed., Materials research forum, Millersville, USA, 2018, pp 10. https://doi.org/10.21741/9781945291555.

[4] U. Ahmadu, A. Muazu, S. Umar, Physical properties of porous pure and Zr/Sn-doped nanocrystalline $BaTiO_3$ ceramics, in: U.M. Basheer Al-Naib (Ed.), Recent Advances. Porous Ceramics, IntechOpen Ltd, London, UK, 2018, pp. 147–170. https://doi.org/10.5772/intechopen.75500.

[5] B. Garbarz-Glos, K. Bormanis, D. Sitko, Effect of Zr Doping on the Electrical Properties of $BaTiO_3$ Ceramics. Ferro. 417(2011)118–123. https://doi.org/10.1080/00150193.2011.578508.

[6] T. Maiti, R. Guo, A.S. Bhalla, Evaluation of experimental resume of $BaZr_xTi_{1-x}O_3$ with perspective to ferroelectric relaxor family: An overview. Ferro., 425(2011)4–26. https://doi.org/10.1080/00150193.2011.644168.

[7] T. Maiti, R. Guo, A.S. Bhalla, Structure-Property Phase Diagram of $BaZr_xTi_{1-x}O_3$ System, J. Am. Ceram. Soc., 91(2008)1769–1780. https://doi.org/10.1111/j.1551-2916.2008.02442.x.

[8] N. Nanakorn, P. Jalupoom, N. Vaneesorn, A. Thanaboonsombut, Dielectric and ferroelectric properties of $Ba(Zr_xTi_{1-x})O_3$ ceramics. Ceram. Int., 34(2008)779–782. https://doi.org/10.1016/j.ceramint.2007.09.024.

[9] S.J. Kuang, X.G. Tang, L.Y. Li, Y.P. Jiang, Q.X. Liu, Influence of Zr dopant on the dielectric properties and Curie temperatures of $Ba(Zr_xTi_{1-x})O_3$ ($0 \leq x \leq 0.12$) ceramics. Scrip. Mat. 61(2009)68–71. https://doi.org/10.1016/j.scriptamat.2009.03.016.

[10] T. Maiti, R. Guo, R., A. S. Bhalla, 2007. Enhanced electric field tunable dielectric properties of $BaZr_xTi_{1-x}O_3$ relaxor ferroelectrics. Appl. Phys. Lett. 90, 182901. https://doi.org/10.1063/1.2734922.

[11] P.S. Dobal, A. Dixit, R.S. Katiyara, Z. Yu, R. Guo, A.S. Bhalla, Micro-Raman scattering and dielectric investigations of phase transition behavior in the $BaTiO_3$–$BaZrO_3$ system. J. Appl. Phys. 89(2001)8085-8091. https://doi.org/10.1063/1.1369399.

[12] D. Hennings, A. Schnell, G. Simon, Diffuse Ferroelectric Phase Transitions in $Ba(Ti_{1-y}Zr_y)O_3$ Ceramics. J. Am. Ceram Soc., 65(1982) 539–544. https://doi.org/10.1111/j.1151-2916.1982.tb10778.x.

[13] J. Ravez, A. Simon, Temperature and Frequency Dielectric Response of Ferroelectric Ceramics with Composition $Ba(Ti_{1-x}Zr_x)O_3$. Eur. J. Sol. Inorg Chem. 34(1997), 1199–1209.

[14] M.H. Frey D.A. Payne, Grain-size effect on structure and phase transformations for barium titanate. Phys. Rev. B 54 (1996) 3158–3168. https://doi.org/10.1103/PhysRevB.54.3158.

[15] T.T. Fang, H.-L. Hsieh, F.-S. Shiau, Effects of Pore Morphology and Grain Size on the Dielectric Properties and Tetragonal–Cubic Phase Transition of High-Purity Barium

Titanate. J. Am. Ceram Soc., 76(1993)1205–1211. https://doi.org/10.1111/j.1151-2916.1993.tb03742.x.

[16] X.G. Tang, J. Wang, X.X. Wang, H.L.W. Chan, Effects of grain size on the dielectric properties and tunabilities of sol–gel derived $Ba(Zr_{0.2}Ti_{0.8})O_3$ ceramics. Sol. Comm. 131 (2004)163–168. https://doi.org/10.1016/j.ssc.2004.05.016.

[17] M. Aghayan, A.K. Zak, M. Behdani, A.M. Hashim, Sol–gel combustion synthesis of Zr-doped $BaTiO_3$ nanopowders and ceramics: dielectric and ferroelectric studies, Ceram. Int. 40 (2014)16141–16146. https://doi.org/10.1016/j.ceramint.2014.07.045.

[18] M. Deluca, C.A. Vasilescu, A.C. Ianculescu, D.C. Berger, C.E. Ciomaga, L.P. Curecheriu, L. Stoleriu, A. Gajovic, L. Mitoseriu, C. Galassi, Investigation of the composition-dependent properties of $BaTi_{1-x}Zr_xO_3$ ceramics prepared by the modified Pechini method, J. Eur. Ceram. Soc. 32(2012)3551–3566. http://dx.doi.org/10.1016/j.jeurceramsoc.2012.05.007.

[19] T. Badapanda, S. Chaterjee, A. Mishra, R. Ranjan, S. Anward, Electric field induced strain, switching and energy storage behaviour of lead free barium zirconium titanate ceramic, Phys. B 521(2017)264–269. https://doi.org/10.1016/j.physb.2017.07.013.

[20] M.L.V. Mahesh, V.V.B. Prasad, A.R. James, Effect of sintering temperature on the microstructure and electrical properties of zirconium doped barium titanate ceramics, *J* Mat. Sci: Mat. Electron 24(2013)4684–4692. https://doi.org/10.1007/s10854-013-1460–3.

[21] P. Julphunthong, T. Bongkarn, Phase formation, microstructure and dielectric properties of $Ba(Zr_{0.1}Ti_{0.9})O_3$ ceramics prepared via the combustion technique. Cur. Appl. Phys. 11 (2011)S60–S65.

[22] A. Ahmad, K.A. Razak, 2017. Synthesis of $BaTiO_3$ and $Ba(Zr_xTi_{1-x})O_3$ by using the soft combustion method. AIP Conf. Proc. 1865, 060001. https://doi.org/doi: 10.1063/1.4993377.

[23] H. Maiwa, Electromechanical properties of $Ba(Zr_{0.2}Ti_{0.8})O_3$ ceramics prepared by spark plasma sintering. Ceram. Int 38(2012)S219-S223. https://doi.org/10.1016/j.ceramint.2011.04.087.

[24] G. Philippot, M. Albino, U.-C. Chung, M. Josse, C. Elissalde, M. Maglione, C. Aymonier, Continuous $BaTi_{1-y}Zr_yO_3$ ($0 \leq y \leq 1$) nanocrystals synthesis in supercritical fluids for nanostructured lead-free ferroelectric ceramics. Mat. Des. 86(2015)354–360. https://doi.org/10.1016/j.matdes.2015.07.111.

[25] B. Liu, Y. Wu, Y.H. Huang, K. X. Song, Y.J. Wu, Enhanced dielectric strength and energy storage density in $BaTi_{0.7}Zr_{0.3}O_3$ ceramics via spark plasma sintering, J Mater Sci. 54(2019)4511–4517. https://doi.org/10.1007/s10853-018-3170-y.

[26] R. Orrù, R. Licheri, A.M. Locci, A. Cincotti, G. Cao, Consolidation/synthesis of materials by electric current activated/assisted sintering. Mater. Sci. Eng. R 63(2009)127–287. https://doi.org/10.1016/j.mser.2008.09.003.

[27] H. Maiwa, Dielectric and Electromechanical Properties of $Ba(Zr_xTi_{1-x})O_3$ (x = 0.1 and 0.2) Ceramics Prepared by Spark Plasma Sintering, Jap. J. Appl. Phys.46(2007)7013–7017. https://doi.org/10.1143/JJAP.46.7013.

[28] A. Varma, A.S. Rogachev, A.S. Mukasyan, S. Hwang, Combustion Synthesis of Advanced Materials: Principles and Applications. Adv. Chem. Eng. 24(1998)79–226. https://doi.org/10.1016/S0065-2377(08)60093-9.

[29] A. Cincotti, R. Licheri, A.M. Locci, R. Orrù, G. Cao, A review on combustion synthesis of novel materials: Recent experimental and modeling results. J. Chem. Tech. Biot. 78(2003)122–127. https://doi.org/10.1002/jctb.757.

[30] B.N. Ezealigo, R. Orrù, F. Torre, P.C. Ricci, F. Delogu, G. Cao, Annealing effects on the structural and optical properties of undoped and Zr-doped Ba titanate prepared by self-propagating high-temperature synthesis. Ceram. Int. 46(11) (2020) 17307-17314. https://doi.org/10.1016/j.ceramint.2020.04.019.

[31] L. Lutterotti, R. Ceccato, R. Dal Maschio, F. Pagani, Quantitative analysis of silicate glass in ceramic materials by the Rietveld method. Mater Sci Forum. 278–281 (1998) 87 https://doi.org/10.4028/www.scientific.net/MSF.278-281.87.

[32] S.K. Rout, L.S. Cavalcante, J.C. Sczancoski, T. Badapanda, S. Panigrahi, M.S. Li, Photoluminescence property of $Ba(Zr_{0.25}Ti_{0.75})O_3$ powders prepared by solid state reaction and polymeric precursor method, Phys. B: Condens. Matter, 404(2009)3341-3347. https://doi.org/10.1016/j.physb.2009.05.014.

[33] T. Badapanda, S. Sarangi, B. Behera, P.K. Sahoo, S. Anwar, T.P. Sinha, G.E. Luz Jr., E. Longo, L.S. Cavalcante, Structural refinement, optical and ferroelectric properties of microcrystalline $Ba(Zr_{0.05}Ti_{0.95})O_3$ perovskite. Curr. Appl. Phys., 14(2014)708-715.https://doi.org/10.1016/j.cap.2014.02.015.

[34] N. Sawangwan, J. Barrel, K. Mackenzie, T. Tunkasiri, The Effect of Zr Content on Electrical Properties of $Ba(Ti_{1-X}Zr_x)O_3$ Ceramics. Appl. Phys. A 90(2008)723–727. https://doi.org/10.1007/s00339-007-4342-9.

[35] S. Mahajan, O.P. Thakur, C. Prakash, K. Sreenivas, Effect of Zr on dielectric, ferroelectric and impedance properties of $BaTiO_3$ ceramic. Bull Mat. Sci., 34(2011)1483–1489. https://doi.org/10.1007/s12034-011-0347-2.

[36] P. Sateesh, J. Omprakash, G.S. Kumar, G. S., G. Prasad, 2015. Studies of phase transition and impedance behavior of $Ba(Zr,Ti)O_3$ ceramics, *J. Adv. Dielectrics*, 5, 1550002. https://doi.org/ 10.1142/S2010135X15500022.

[37] F. Benaballah, A. Simon, H. Khemakhem, C. Elissalde, M. Maglione, 2011. Linking large piezoelectric coefficients to highly flexible polarization of lead free $BaTiO_3$-$CaTiO_3$-$BaZrO_3$ ceramics. J. Appl. Phys. 109, 124116. https://doi.org/10.1063/1.3599854.

[38] C.A. Schneider, W.S Rasband, K.W. Eliceiri, NIH Image to Image J: 25 years of image analysis. Nat. methods 9(7) (2012)671-675. https://doi.org/doi: 10.1038/nmeth.2089.

[39] Z. Yu, C. Ang, R. Guo, A.S. Bhalla, Piezoelectric and strain properties of $Ba(Ti_{1-x}Zr_x)O_3$ ceramics. J. Appl. Phys. 92(2002)1489–1493. https://doi.org/10.1063/1.1487435.

[40] P. Zheng, J.L. Zhang, S.F. Shao, Y.Q. Tan, C.L. Wang, Piezoelectric properties and stabilities of CuO-modified ceramics. Appl. Phys. Lett. 94(2009)032902. https://doi.org/10.1063/1.3072347.

[41] T.L. Jordan and Z. Ounaies, Piezoelectric Ceramics Characterization, NASA, Langley Research Center Hampton, Virginia, 2001, https://apps.dtic.mil/dtic/tr/fulltext/u2/a395517.pdf

[42] P.A. Jha, A.K. Jha, Effect of sintering temperature on the grain growth and electrical properties of barium zirconate titanate ferroelectric ceramics. J Mat. Sci: Mat. Electron 24(2013)1511–1518. https://doi.org/10.1007/s10854-012-0963-7.

[43] Z. Sun, Y. Pun, Z. Dong, Y. Hu, X. Liu, P. Wang, Effect of Zr^{4+}content on the T_C range and dielectric and ferroelectric properties of $BaZr_xTi_{1-x}O_3$ ceramics prepared by microwave sintering. Ceram. Int. 40 (2014) 3589–3594, http://dx.doi.org/10.1016/j.ceramint.2013.09.069.

[44] C. Fu, F. Pan, W. Cai, X. Deng, X. Liu, 2009. Microstructures and dielectric properties of $BaZr_{0.2}Ti_{0.8}O_3$ ceramics. J Phys. Conf. Ser. 152, 012075. https://doi.org/10.1088/1742-6596/152/1/012075.

[45] W. Cai, J. Gao, M. Zhang, C. Fu, Effect of sintering temperature on diffuse phase transition of barium zirconate titanate ceramics. Int. Ferro. 105 (2009) 1–10. https://doi.org/10.1080/10584580903034548.

[46] Z. Yu, R. Guo, A.S. Bhalla, Dielectric behavior of $Ba(Ti_{1-x}Zr_x)O_3$ single crystals, J. Appl. Phys. 88 (2000)410–415. https://doi.org/10.1063/1.373674.

[47] L. Dong, D.S. Stone, R.S. Lakes, Enhanced dielectric and piezoelectric properties of $xBaZrO_3$-(1-x)$BaTiO_3$ ceramics, 2012. J Appl. Phys. 111, 084107 http://dx.doi.org/10.1063/1.4705467.

[48] F. Moura, A.Z. Simões, B.D. Stojanovic, M.A. Zaghete, E. Longo, J.A. Varela, Dielectric and ferroelectric characteristics of barium zirconate titanate ceramics prepared from mixed oxide method, J. Alloys and Compds 462(2008)129–134. http://dx.doi.org/10.1016/j.jallcom.2007.07.077.

[49] A.K. Kalyani, K. Brajesh, A. Senyshyn, R. Ranjan, 2014. Orthorhombic-tetragonal phase coexistence and enhanced piezo-response at room temperature in Zr, Sn, and Hf modified $BaTiO_3$. Appl. Phys. Lett. 104, 252906. https://doi.org/10.1063/1.4885516.

[50] S.-J. Jeong, D.-S. Lee, E.-C. Park, J.-S. Song, Piezoelectric properties of a $Ba(Zr_{0.075}Ti_{0.925})O_3$ single crystal induced by poling treatment. J Electroceram, 17(2006)537–541. https://doi.org/10.1007/s10832-006-7724-z.

[51] W. Li, Z. Xu, R. Chu, P. Fu, G. Zang, Dielectric and piezoelectric properties of $Ba(Zr_xTi_{1-x})O_3$ lead-free ceramics. Braz. J. Phys. 40(2010)353–356. http://dx.doi.org/10.1590/S0103-97332010000300018.

Figures

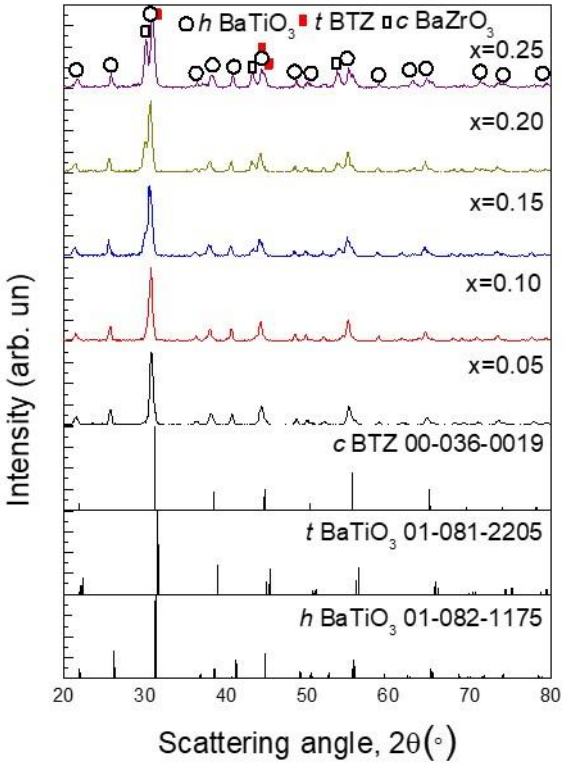

Figure 1: Room temperature XRD patterns of powders obtained by SHS for different *x* values (cf. Eq. 1).

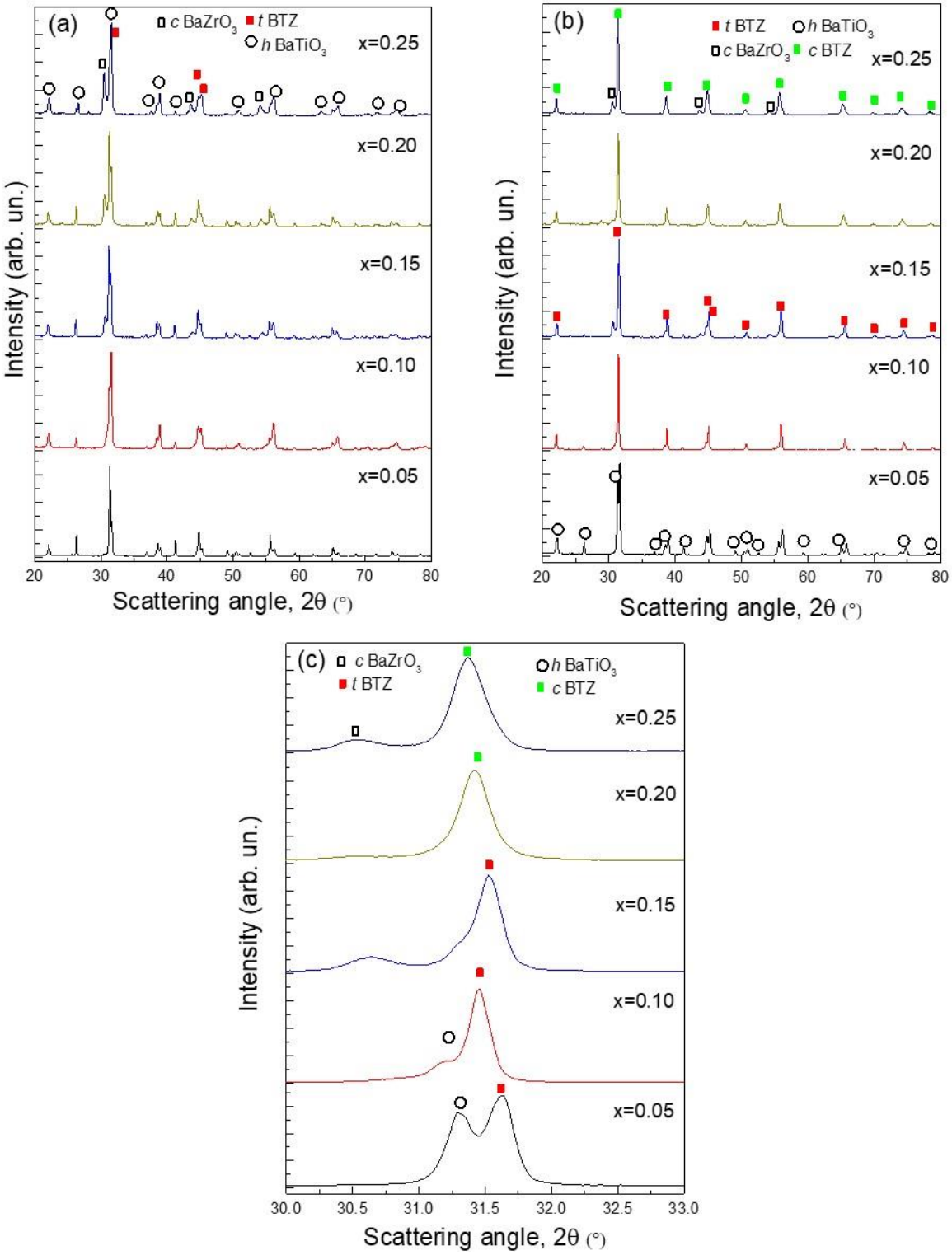

Figure 2: XRD patterns of BTZ ceramics obtained by SPS at (a) T_D= 1200ºC, (b) T_D= 1400°C, (c) Zoomed view of (b).

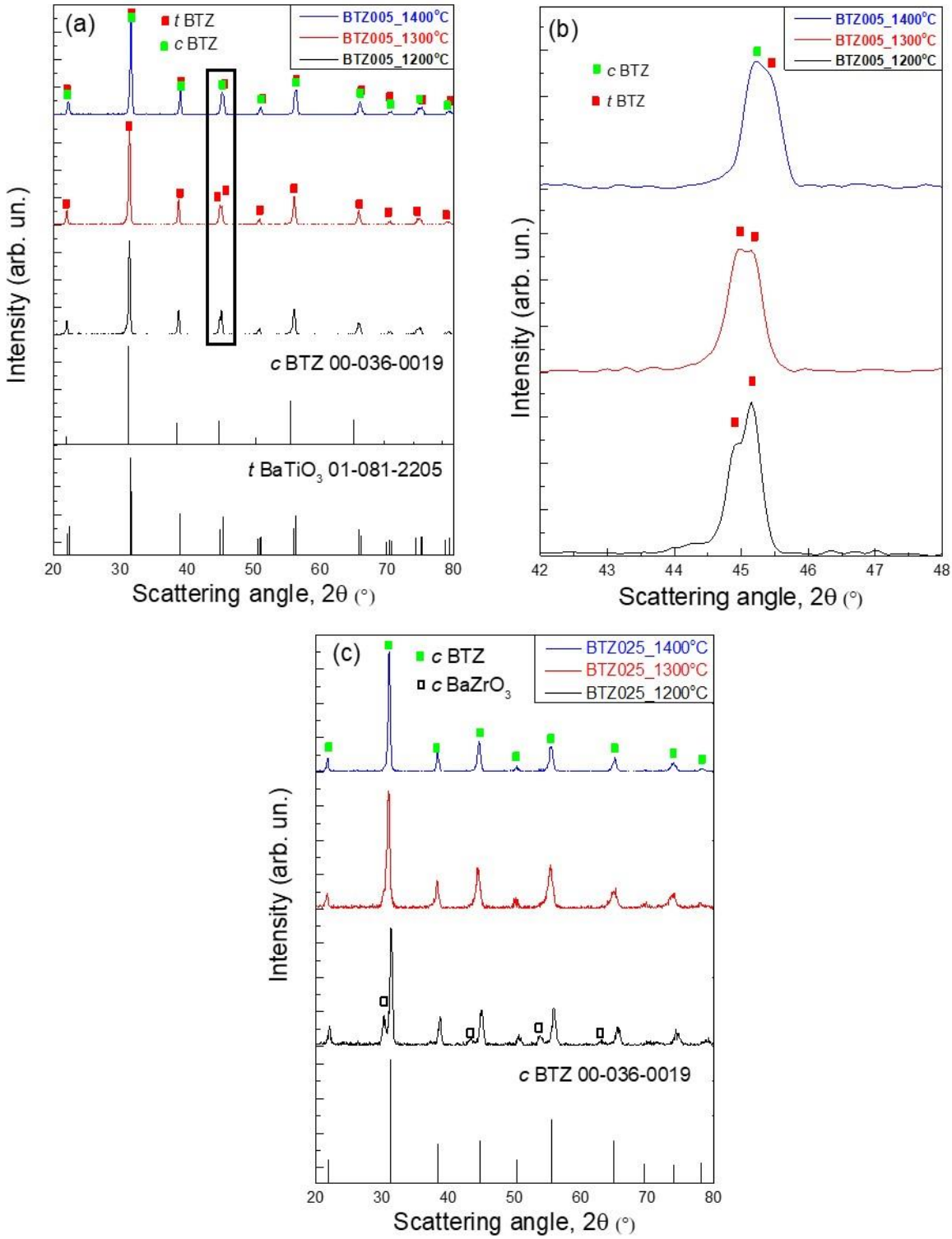

Figure 3: XRD patterns of (a)-(b) BTZ005, and (c) BTZ025 ceramics obtained by SPS (T_D=1200, 1300, and 1400°C) after being post annealed for 3h at 1200°C.

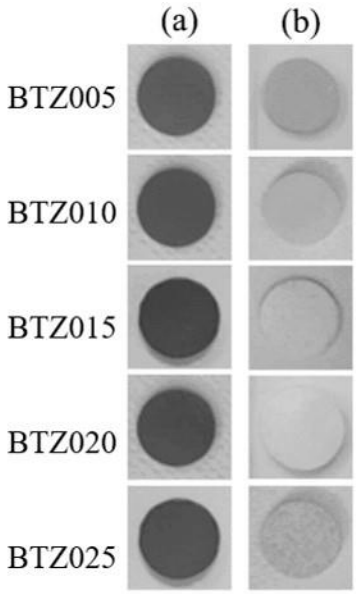

Figure 4: Images of $BaTi_{(1-x)}Zr_xO_3$ *(x=0.05–0.25)* ceramics sintered by SPS at 1400°C before (a) and after (b) post-annealing at 1200°C for 3h.

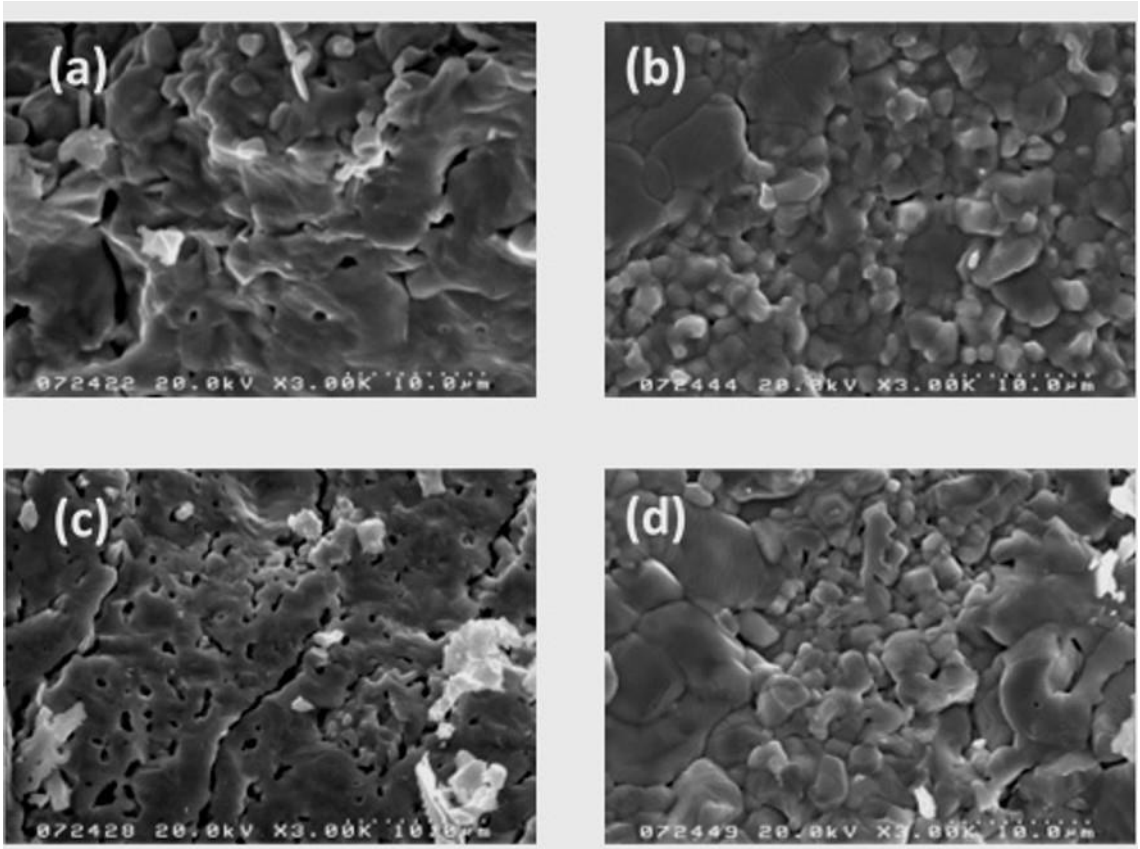

Figure 5: Fractured surfaces of BTZ ceramics obtained by SPS and subsequently annealed at 1200ºC for 3h: (a) BTZ005, T_D=1200°C; (b) BTZ005, T_D=1400°C; (c) BTZ025, T_D=1200°C; (d) BTZ025, T_D=1400°C.

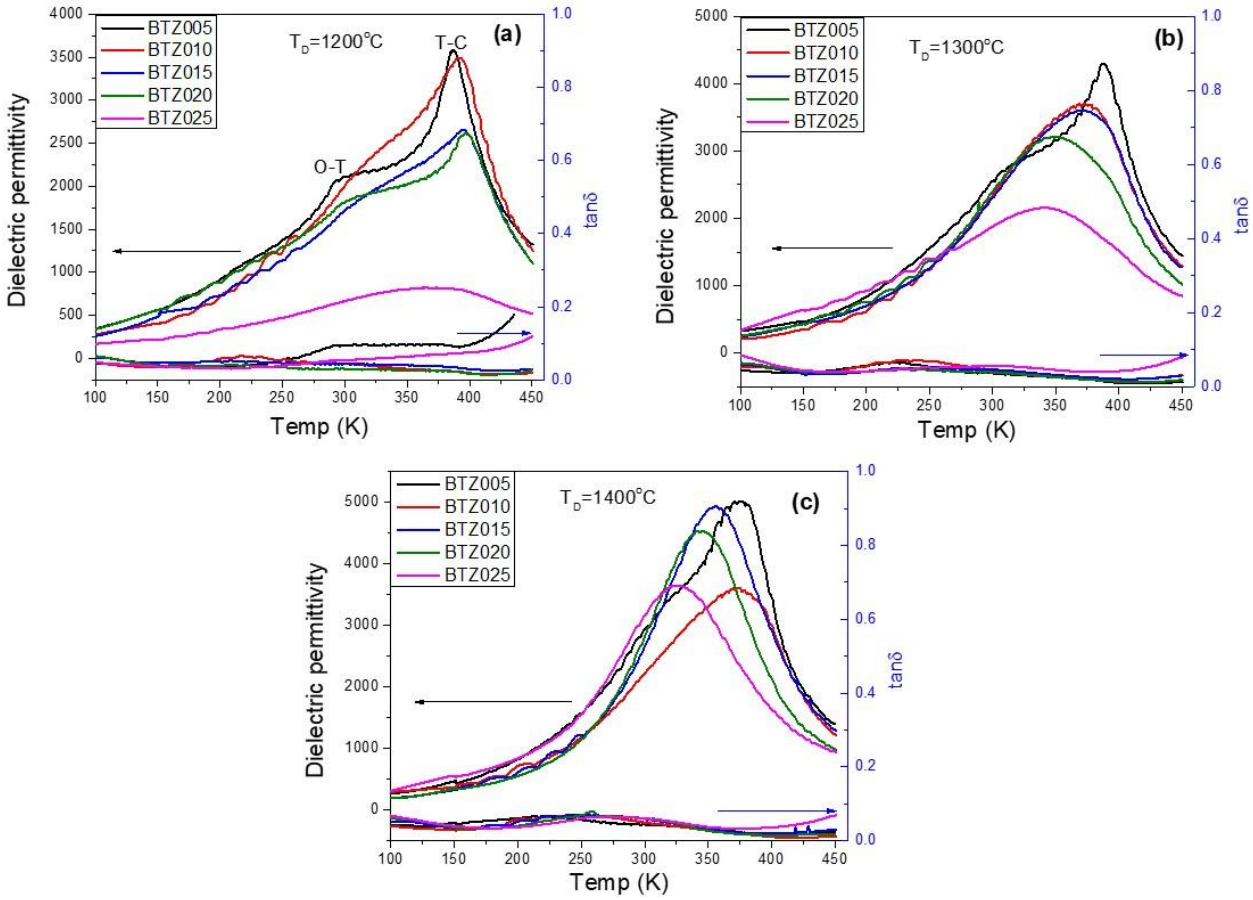

Figure 6: Dielectric permittivity and loss (1kHz) of $BaTi_{(1-x)}Zr_xO_3$ *(x=0.05–0.25)* ceramics: (a) T_D=1200°C, (b) T_D=1300°C, and (c) T_D=1400°C. All samples were post-annealed for 3h at 1200ºC. (O= orthorhombic; T= tetragonal; C=cubic phase transition)

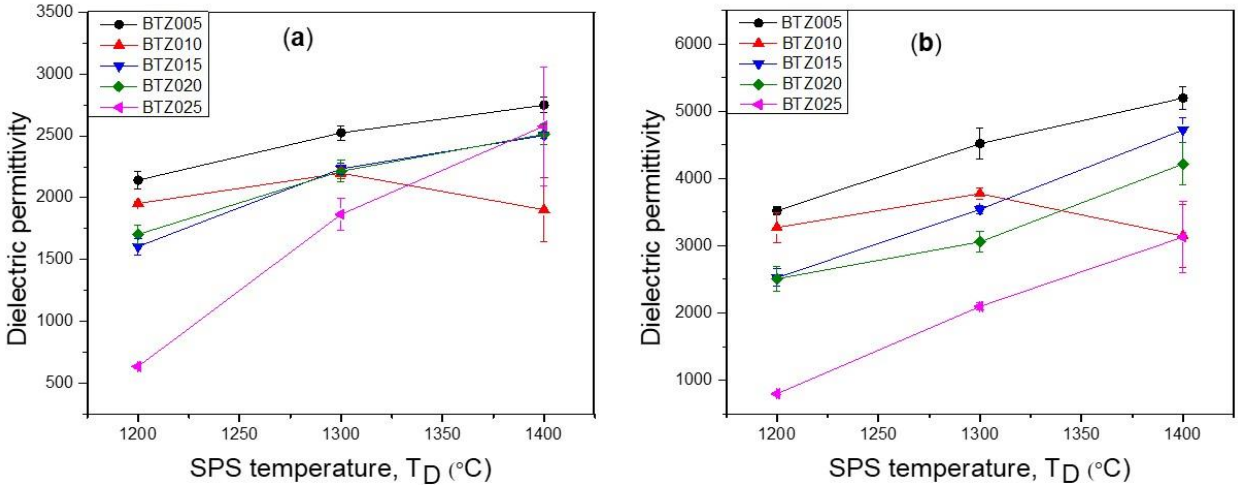

Figure 7: Dielectric permittivity at (a) room (25ºC) and (b) Curie (T_c) temperature of $BaTi_{(1-x)}Zr_xO_3$ *(x=0.05–0.25)* ceramics as a function of T_D.

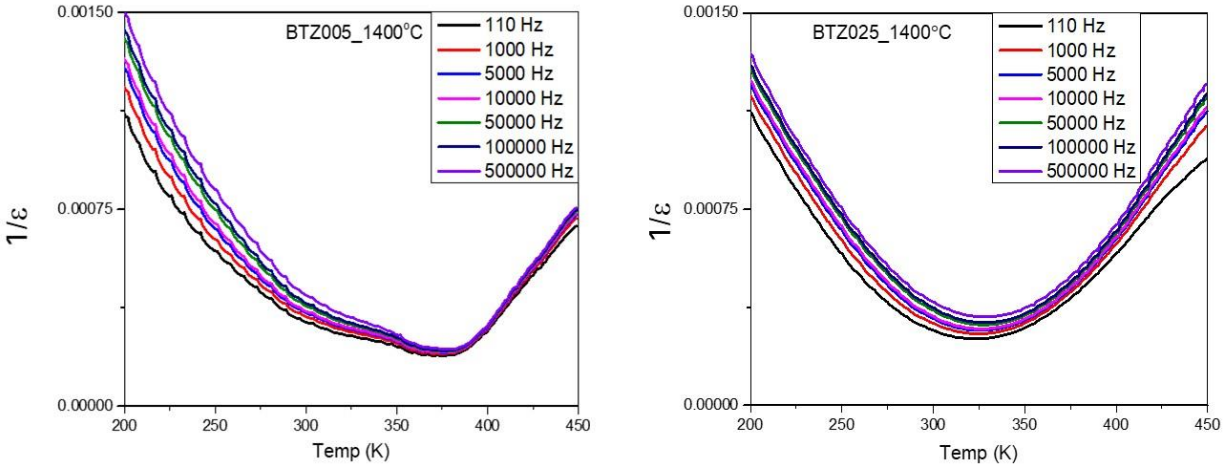

Figure 8: Curie-Weiss plots of $BaTi_{(1-x)}Zr_xO_3$ *(x=0.05 and 0.25)* ceramics sintered at 1400°C and subsequently post-annealed at 1200°C for 3h.

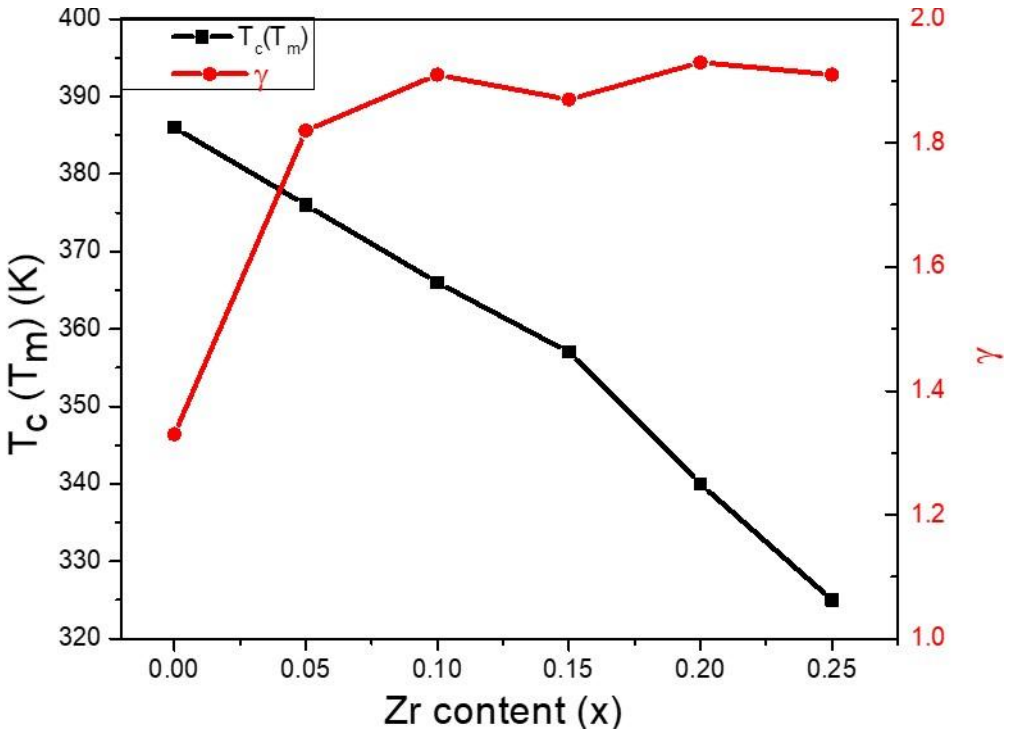

Figure 9: Plot of T_c (T_m) at 1 kHz and diffuseness coefficient (γ) as a function of Zr content for ceramics sintered at 1400°C and subsequently post-annealed at 1200°C for 3h.

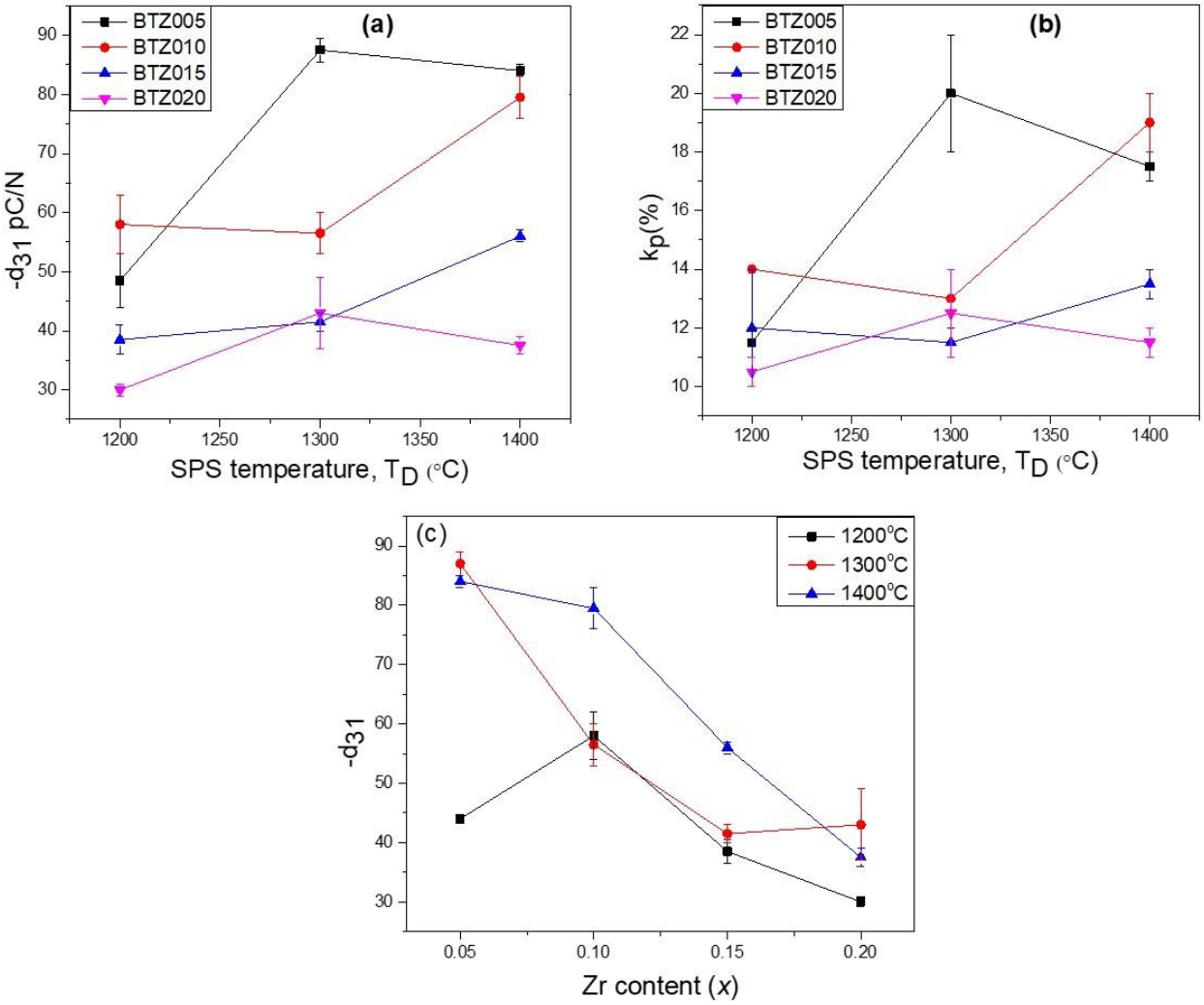

Figure 10: Piezoelectric properties of BTZ ceramics annealed at 1200ºC for 3h. **(a)** Piezoelectric charge coefficient (d_{31}) and **(b)** planar coupling factor (k_p) as a function of sintering temperature; **(c)** piezoelectric charge coefficient (d_{31}) as a function of Zr content.

Supplementary Material

Influence of the Spark Plasma Sintering temperature on the structure and dielectric properties of $BaTi_{(1-x)}Zr_xO_3$ ceramics

Blessing N. Ezealigo[1], Roberto Orrù[1,*], Catherine Elissalde[2,*], Hélène Debéda[3], U-Chan Chung[2], Mario Maglione[2], Giacomo Cao[1]

[1]*Dipartimento di Ingegneria Meccanica, Chimica e dei Materiali, Unità di Ricerca del Consorzio Interuniversitario Nazionale per la Scienza e Tecnologia dei Materiali (INSTM) - Università degli Studi di Cagliari, via Marengo 2, 09123 Cagliari, Italy*

[2]*Université de Bordeaux, CNRS, ICMCB, UMR 5026, 87 avenue du Dr A. Schweitzer, 33608 Pessac, France*

[3]*Université de Bordeaux, Laboratoire IMS, UMR 5218, 351 Cours de la Libération, 33405 Talence, Cedex, France*

Corresponding author: Roberto Orrù (roberto.orru@dimcm.unica.it); Catherine Elissalde (catherine.elissalde@icmcb.cnrs.fr)

Supplementary Tables S1-S4

Supplementary Figure S1-S5

Table S1: Phases and quantitative phase analysis results (Rietveld procedure) of post annealed BTZ005 (T_D=1200°C and T_D=1400°C) and BTZ025 (T_D=1400°C) samples.

BTZ005 (T_D=1200°C)			
Phase	**a (Å)**	**c (Å)**	**Wt. (%)**
Tetragonal P4mm ($BaTiO_3$)	3.998	4.022	87.5
Cubic Pm-3m ($BaTiO_3$)	4.056	/	12.5
BTZ005 (T_D=1400°C)			
Phase	**a (Å)**	**c (Å)**	**Wt. (%)**
Tetragonal P4mm ($BaTiO_3$)	3.995	4.024	70.3
Cubic Pm-3m ($BaTiO_3$)	4.017	/	29.7
BTZ025 (T_D=1400°C)			
Phase	**a (Å)**	**c (Å)**	**Wt. (%)**
Cubic Pm-3m ($BaTiO_3$)	4.040	/	100

Table S2: Dielectric characteristics at 1kHz of $BaZr_xTi_{(1-x)}O_3$ *(x=0.05–0.25)* ceramics. T_D values are indicated below samples ID.

Sample ID	**Dielectric constant at room temperature**	**Dielectric constant at Curie temperature**	**tan δ at room temperature**	**tan δ at Curie temperature**
BTZ005 1200°C	2142±73	3521±56	0.041	0.031
BTZ005 1300°C	2524±57	4518±228	0.039	0.016
BTZ005 1400°C	2749±63	5195s±172	0.044	0.020
BTZ010 1200°C	1954±15	3269±218	0.044	0.021
BTZ010 1300°C	2199±42	3775±82	0.048	0.024
BTZ010 1400°C	1903±256	3145±465	0.053	0.015
BTZ015 1200°C	1606±67	2525±129	0.043	0.023
BTZ015 1300°C	2234±45	3541±61	0.046	0.027
BTZ015 1400°C	2503±26	4721±181	0.059	0.030
BTZ020 1200°C	1703±75	2510±182	0.031	0.020
BTZ020 1300°C	2215±86	3057±150	0.039	0.028
BTZ020 1400°C	2514±83	4216±314	0.058	0.032
BTZ025 1200°C	635±17	799±21	0.067	0.078
BTZ025 1300°C	1866±127	2097±57	0.055	0.048
BTZ025 1400°C	2579±480	3128±525	0.063	0.052

Table S3: Curie temperature, Curie-Weiss temperature, temperature of deviation from Curie-Weiss law, Curie constant, and diffuseness coefficient values of $BaZr_xTi_{(1-x)}O_3$ ceramics. T_D values are indicated below samples ID.

Sample ID	**T_c (T_m) (K)**	**T_o (K)**	**T_{cw} (K)**	**Curie constant (K^{-1}) x10^5**	**γ**
BTZ005 1200°C	386	361	399	1.22	1.42
BTZ005 1300°C	386	370	401	1.39	1.69
BTZ005 1400°C	378	368	401	1.23	1.82
BTZ010 1200°C	390	373	408	1.02	1.71
BTZ010 1300°C	369	362	403	1.31	1.83
BTZ010 1400°C	366	360	403	1.11	1.85
BTZ015 1200°C	393	367	415	0.98	1.81
BTZ015 1300°C	370	374	410	1.12	1.86
BTZ015 1400°C	350	361	402	1.30	1.83
BTZ020 1200°C	396	371	417	0.97	1.66
BTZ020 1300°C	347	360	406	0.94	1.86
BTZ020 1400°C	341	356	397	1.14	1.9
BTZ025 1200°C	374	322	421	0.69	1.92
BTZ025 1300°C	338	337	401	0.94	1.93
BTZ025 1400°C	331	314	360	1.04	1.95

*T_c = transition temperature or Curie temperature; T_m= temperature at maximum permittivity; T_{cw}= Temperature from which the permittivity starts to deviate from Curie-Weiss law; T_o= Curie-Weiss temperature

Table S4: Piezoelectric characteristics and density values of $BaZr_xTi_{(1-x)}O_3$ ceramics prepared by SHS and sintered by SPS (T_D values are indicated below samples ID). Literature data are also reported for the sake of comparison

Sample ID	**Density (g/cm^3)**	Q_m	k_p **(%)**	$-d_{31}$ **(pC/N)**	**Ref**
BTZ005 1200°C	5.43	181	11.5±0.5	48.5±4.5	This work
BTZ005 1300°C	5.89	81	20±2	87.5±2	This work
BTZ005 1400°C	5.57	79	17.5±0.5	84±1	This work
BTZ010 1200°C	5.51	137	14	58±5	This work
BTZ010 1300°C	5.64	181	13±1	56.5±3.5	This work
BTZ010 1400°C	5.47	57	19±1	79.5±3.5	This work
BTZ015 1200°C	5.65	130	12±2	38.5±2.5	This work
BTZ015 1300°C	5.77	196	11.5±0.5	41.5±1.5	This work
BTZ015 1400°C	5.78	138	13.5±05	56±1	This work
BTZ020 1200°C	5.38	193	10.5±0.5	30±1	This work
BTZ020 1300°C	5.50	128	12.5±1.5	43±6	This work
BTZ020 1400°C	5.84	178	11.5±0.5	37.5±1.5	This work
BTZ020 1100°C	5.83	312	25	126	[23]
BTZ005 1500°C	5.80	-	-	64	[39]
BTZ004 1450°C	5.86	180	42.1	90	[40]

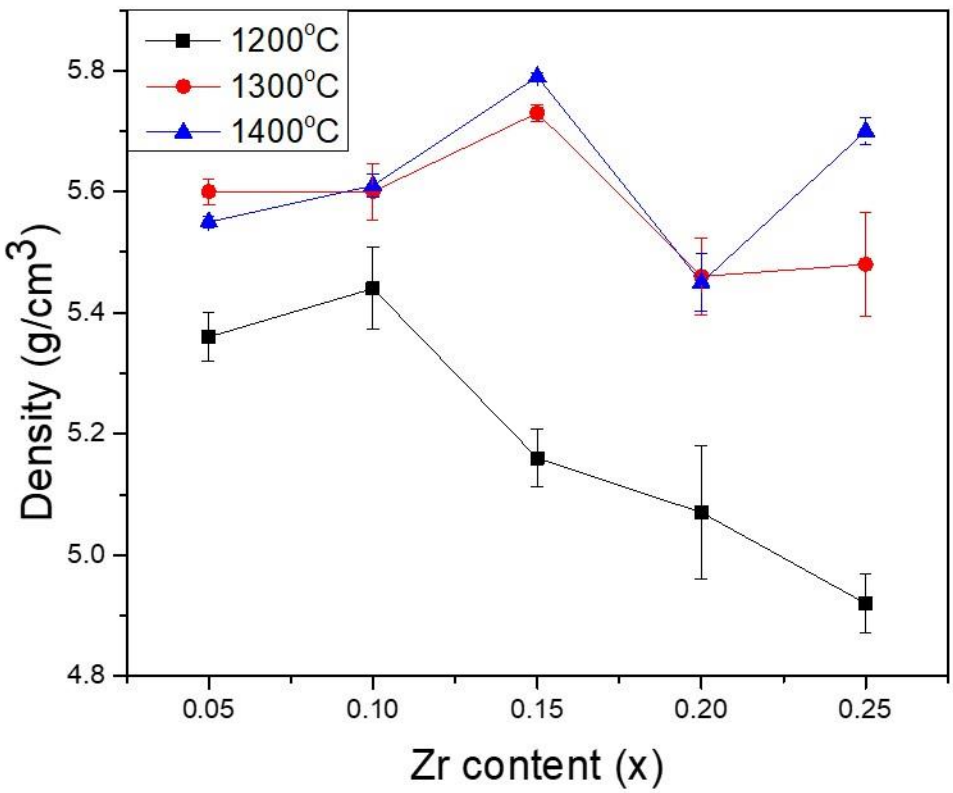

Figure S1: Density of post-annealed BTZ ceramics (T_D=1200−1400℃) as a function of Zr content.

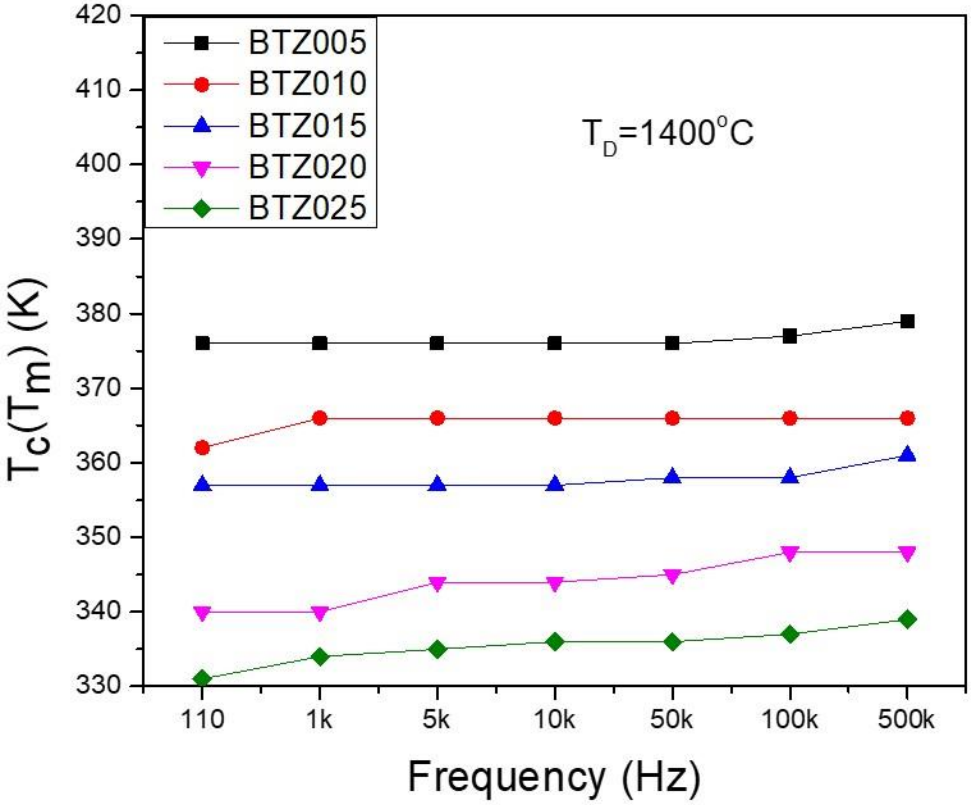

Figure S2: Curie temperature as a function of frequency for different BTZ compositions (T_D 1400°C).

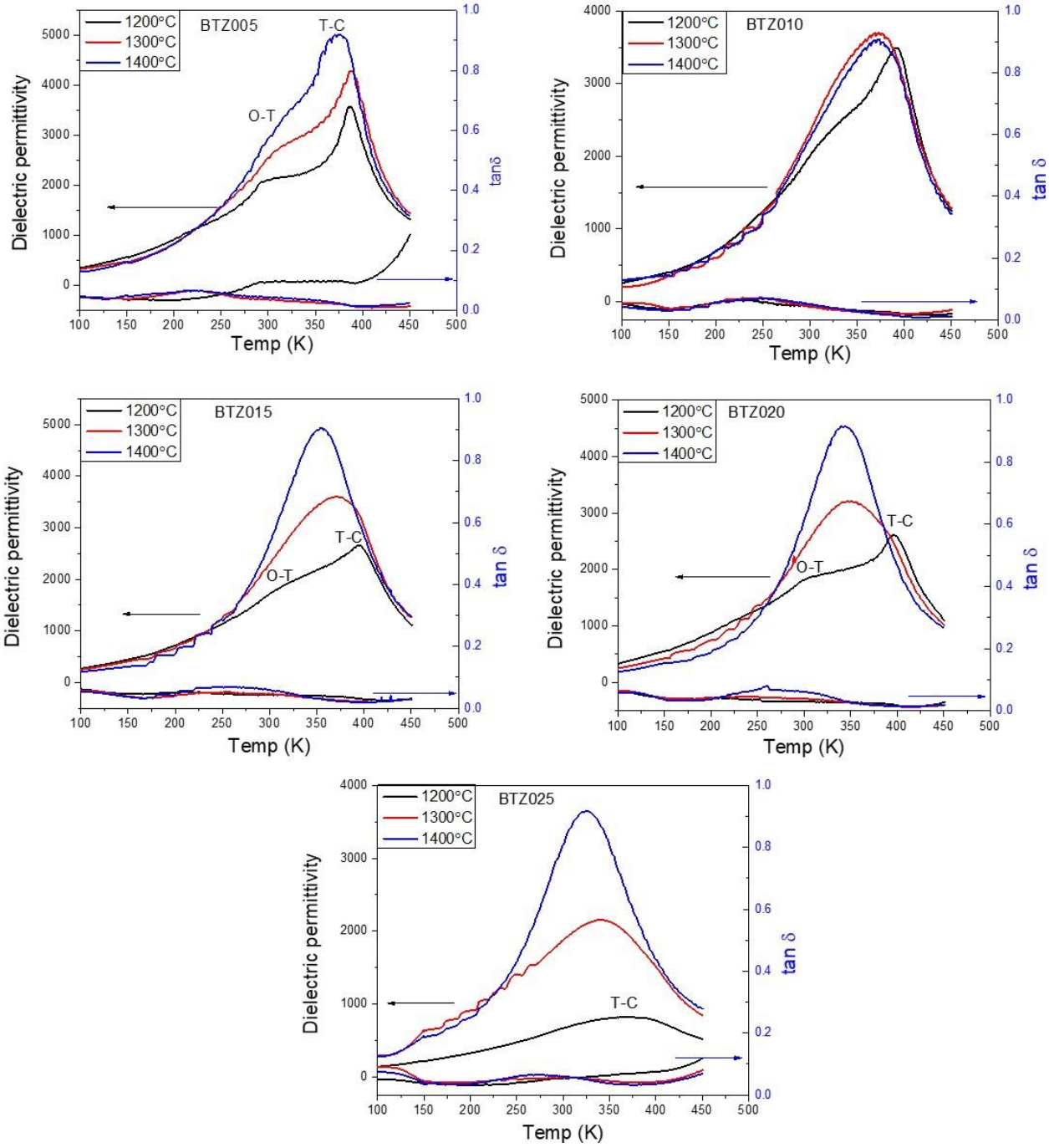

Fig. S3: Dielectric constant and loss of $BaZr_xTi_{(1-x)}O_3$ *(x=0.05-0.25)* ceramics at 1kHz. (O= orthorhombic; T= tetragonal; C=cubic phase transition).

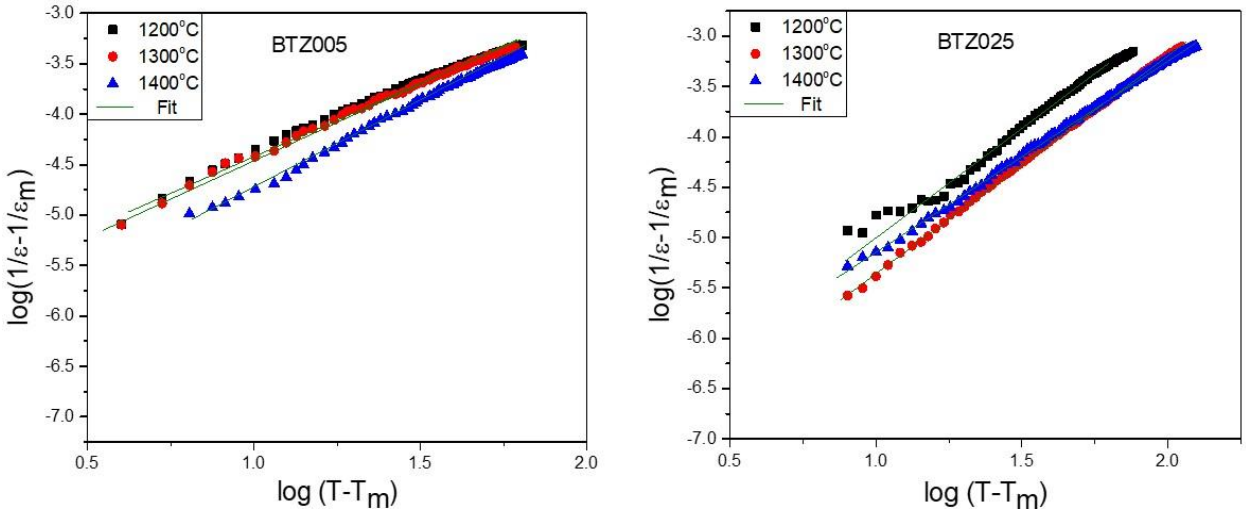

Fig. S4: Plots of $\log(\frac{1}{\varepsilon}-\frac{1}{\varepsilon_m})$ versus $\log(T-T_m)$ for BTZ005 and BTZ025 compositions.

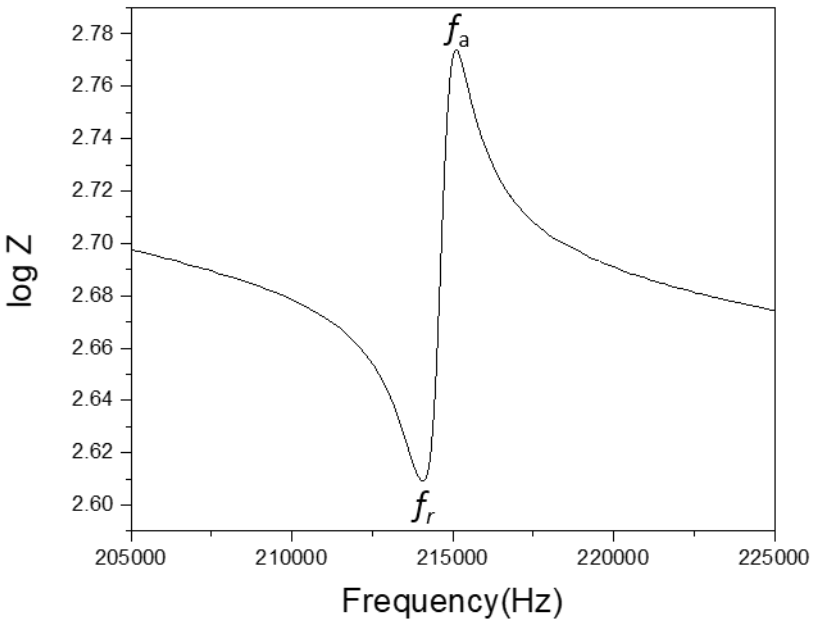

Fig. S5: Impedance as a function of frequency, showing the resonance (f_r) and antiresonance (f_a) frequencies, relative to BTZ005 ceramics sintered at 1300°C.